



● *Original Contribution*

MYOCARDIAL STRETCH POST-ATRIAL CONTRACTION IN HEALTHY VOLUNTEERS AND HYPERTROPHIC CARDIOMYOPATHY PATIENTS

MIHAI STRACHINARU,* MARCEL L. GELEIJNSE,* NICO DE JONG,[†] ANNEMIE VAN DEN BOSCH,*
MICHELLE MICHELS,* AREND F.L. SCHINKEL,* ANTONIUS F.W. VAN DER STEEN,[†]
JOHAN G. BOSCH,[†] and HENDRIK J. VOS[†]

* Department of Cardiology, Erasmus MC, Rotterdam, The Netherlands; and [†] Thoraxcenter Biomedical Engineering, Erasmus MC, Rotterdam, The Netherlands

(Received 14 February 2019; revised 21 March 2019; in final form 29 April 2019)

Abstract—In cardiac high-frame-rate color tissue Doppler imaging (TDI), a wave-like pattern travels over the interventricular septum (IVS) after atrial contraction. The propagation velocity of this myocardial stretch post-atrial contraction (MSPa) was proposed as a measure of left ventricular stiffness. The aim of our study was to investigate the MSPa in patients with hypertrophic cardiomyopathy (HCM) compared with healthy volunteers. Forty-two healthy volunteers and 33 HCM patients underwent high-frame-rate (>500 Hz) TDI apical echocardiography. MSPa was visible in TDI, M-mode and speckle tracking. When assuming a wave propagating with constant velocity, MSPa in healthy volunteers (1.6 ± 0.3 m/s) did not differ from that in HCM patients (1.8 ± 0.8 m/s, $p = 0.14$). Yet, in 42% of patients with HCM, the MSPa had a non-constant velocity over the wall: in the basal IVS, the velocity was lower (1.4 ± 0.5 m/s), and in the mid-IVS, much higher (6.1 ± 3.4 m/s, $p < 0.0001$), and this effect was related to the septal thickness. The reason is hypothesized to be the reaching of maximal longitudinal myocardial distension in HCM patients. (E-mail: m.strachinaru@erasmusmc.nl) © 2019 The Author(s). Published by Elsevier Inc. on behalf of World Federation for Ultrasound in Medicine & Biology. This is an open access article under the CC BY-NC-ND license. (<http://creativecommons.org/licenses/by-nc-nd/4.0/>).

Key Words: Myocardial stretch, Atrial contraction, Stiffness, High-frame-rate tissue Doppler.

INTRODUCTION

The possibility of imaging the heart at very high frame rates has opened a new window to our understanding of cardiac physiology and pathology (Cikes et al. 2014; Voigt et al. 2018). High-frame-rate imaging allows minute tracking of many wave-like phenomena that are either naturally present during the cardiac cycle because of valve closure (Brekke et al. 2014; Kanai 2009; Strachinaru et al. 2017, 2019; Vos et al. 2017) and atrial contraction (Pislaru et al. 2014, 2017; Voigt et al. 2002) or are induced by external sources (Pernot et al. 2011; Song et al. 2016; Vejdani-Jahromi et al. 2017; Villemain et al. 2018a, b). The naturally occurring shear waves secondary to the closure of the valves (Brekke et al. 2014; Strachinaru et al. 2017) appear during intervals in which the muscle is in the process of contraction (mitral valve closure) or relaxation (aortic valve closure), challenging the

physiologic interpretation of the data. Such complexity is absent in late diastole, where the left ventricle (LV) is supposed to be in a quasi-relaxed state, allowing estimation of the true intrinsic elasticity of the wall (Pislaru et al. 2014, 2017; Voigt et al. 2002). A strain rate wave-like pattern visible in the LV myocardium after atrial contraction was reported by Voigt et al. (2002), who estimated its propagation velocity as between 2 and 4.6 m/s in the interventricular septum (IVS) of normal individuals at a frame rate of 178 Hz. They found the value to be preload dependent. Later, Pislaru et al. investigated the same tissue Doppler imaging (TDI) velocity and strain rate pattern at higher frame rates (350–460 Hz) and computed values of 1.4 ± 0.2 m/s in normal individuals and 2.2 ± 0.7 m/s in severe aortic stenosis patients (Pislaru et al. 2014, 2017). Yet, the exact nature and behavior of this tissue velocity-based pattern remain unclear. These earlier studies hypothesized that the fast traction on the mitral annulus by the atrial contraction generates a wave into the LV, which travels from base to apex with a constant velocity that is related to the

Address correspondence to: Mihai Strachinaru, Department of Cardiology, Erasmus MC, Postbus 2040, 3000 CA Rotterdam, The Netherlands. E-mail: m.strachinaru@erasmusmc.nl

underlying tissue stiffness. It is also possible that this wave has a radial component (Pislaru et al. 2017).

The aim of this study was to investigate the nature of the wave-like pattern following atrial contraction by integrating multiple high-frame-rate ultrasound modalities. To further test the above hypothesis we studied both normal and hypertrophic hearts, the latter being supposedly stiffer than normal hearts (Elliott et al. 2014; Mirsky and Parmley 1973; Villemain et al. 2018a, b).

METHODS

In apical TDI videos of the interventricular septal wall, wave patterns after atrial contraction are visible, as further described in the next subsection. The pattern has a propagation velocity on the order of several meters per second (Pislaru et al. 2014, 2017; Voigt et al. 2002), and general theory predicts that waves travel faster in stiffer material (Giorgi 1993). We denote this pattern as myocardial stretch propagation post-atrial contraction (MSPa), in line with a similar definition by Pislaru et al. We started this study with the hypothesis of a wave propagating with constant velocity over the first 4 to 5 cm of the interventricular septum, as previously described in normal and pathologic hearts after atrial contraction (Pislaru et al. 2014, 2017; Voigt et al. 2002).

Study population

This prospective study was conducted in 2016–2017 according to the principles of the Declaration of Helsinki and approved by the Institutional Medical Ethical Committee (MEC-2014-611, MEC-2017-209). Written informed consent was obtained from every participant. The same patient pool was used for selecting the study population in a different work investigating naturally occurring shear waves after valve closure (Strachinaru et al. 2019).

Healthy volunteers aged 18–62 y (N = 42). Patients were excluded if they had a history of cardiovascular disease or systemic disease, a finding of cardiac abnormalities during the examination (including QRS duration >100 ms), cardiovascular risk factors including hypertension (cutoff value: 140/90 mm Hg), diabetes mellitus or hypercholesterolemia, breast implants or were pregnant. Professional athletes or morbidly obese individuals (body mass index >40 kg/m²) were also excluded.

Hypertrophic cardiomyopathy (HCM) patients aged 20 to 73 y, recruited from the HCM outpatient clinic (N = 33). Patients were included if they had a definitive diagnosis of hypertrophic cardiomyopathy (Elliott et al. 2014), with pathologic septal hypertrophy

(end-diastolic thickness >15 mm or >13 mm if diagnosed through family screening) and normal systolic function (ejection fraction >55%). Exclusion criteria were associated coronary artery disease, more than mild valve disease (systolic anterior movement was not considered an exclusion criterion), prior septal reduction (either surgical or interventional) and atrial fibrillation.

Echocardiography

All echocardiographic studies were performed by one experienced sonographer (M.S.). Normal complete echocardiographic studies were performed, including 2-D, Doppler and pulsed-wave TDI of the mitral annulus. The peak velocity of the early diastolic mitral inflow was measured (*E* wave), as was the peak early diastolic tissue velocity of the medial mitral annulus in the apical four-chamber view (*e'* wave). Their ratio (*E/e'*) was then calculated as an index of the early diastolic properties of the LV. We also quantified the motion of the atrioventricular annulus with atrial contraction by measuring peak TDI velocity (*a'* wave) and *a'* acceleration in pulsed wave tissue Doppler images of the medial mitral annulus in the apical four-chamber view. As *a'* acceleration is not a standard clinical measurement, we detailed it in Figure 1.

Normal complete echocardiographic studies were performed as a reference. Grayscale loops were also acquired at the highest frame rate achievable (frame rates of 200–250 Hz) from the IVS in the parasternal and apical four-chamber views.

Tissue velocities of the LV myocardium were sampled in color TDI in standard parasternal and apical four-chamber views using a Philips iE33 system (Philips Medical, Best, The Netherlands) equipped with an S5-1 transducer (three separate recordings for each view, two heartbeats per clip). As previously described (Strachinaru et al. 2017), by carefully tuning the relationship between the depth of the image, the 2-D line density and the TDI field of view, frame rates >500 Hz were achieved in regular clinical TDI mode. The color tissue velocity scale was set up for optimal visualization of the stretch, leading to scale limits between 1.5 and 3.5 cm/s, corresponding to the amplitude of the wave pattern in TDI, which is not to be confused with its propagation velocity, which is orders of magnitude higher.

Figure 2 illustrates the alignment of the probe with respect to the propagation of the wave on the septal wall in the apical four-chamber view. TDI is extremely sensitive to tissue motion in the axial direction of the probe, indicated by the yellow arrows, but not sensitive to lateral motion. We use this directional sensitivity to determine the dominant tissue motion by TDI. Additionally, we analyze grayscale clips with a speckle

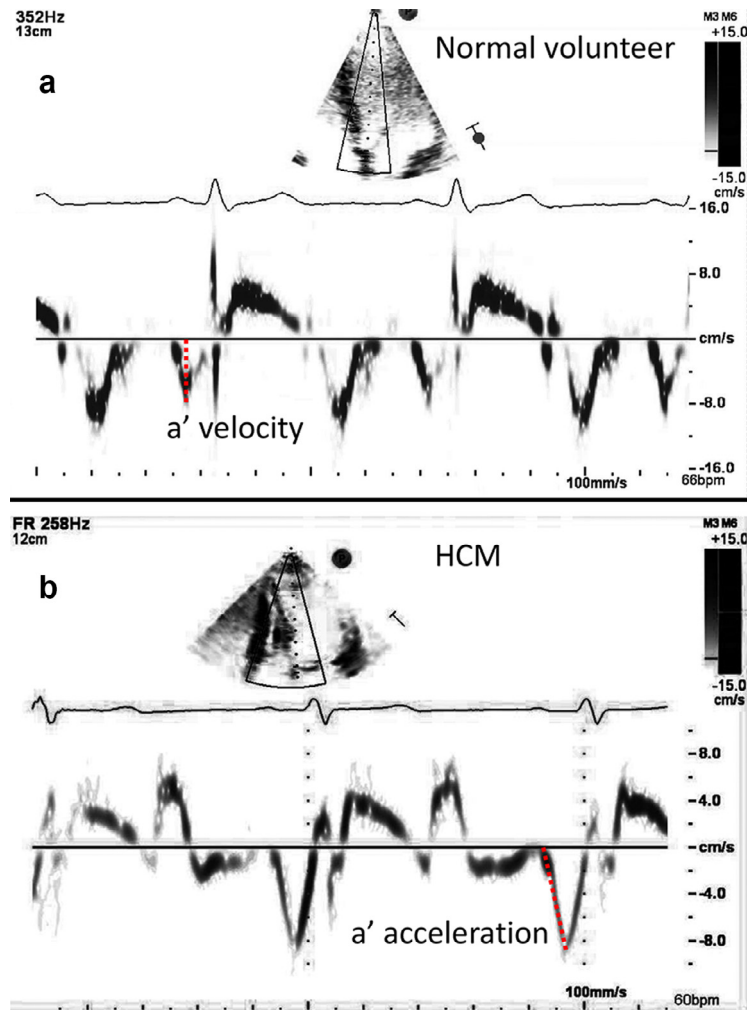


Fig. 1. Clinical pulse-wave tissue Doppler imaging recordings of the medial mitral annulus in the apical four-chamber view, with demonstration of the a' velocity and acceleration slope calculation. (a) Normal healthy volunteer. (b) Patient with hypertrophic cardiomyopathy. Note that the velocity scales for the two recordings differ.

tracking algorithm. Speckle tracking detects motion in all directions, albeit with generally lower frame rate, sensitivity and accuracy than TDI. By combining the information from all modalities, we illustrate the predominant tissue motion after atrial contraction.

The Digital Imaging and Communications in Medicine TDI loops were processed using Qlab 9 (Philips Medical, Best, The Netherlands). As illustrated in Figure 3a and b, the software is used to trace an anatomic M-mode line in the TDI clips. The M-mode line was traced midwall, starting apically and ending at the beginning of the muscular septum, pointing toward the possible wave source (the atrioventricular annulus). The software generates a map of color-coded TDI velocities over time and space, that is, along the M-mode line (Fig. 3c). After atrial contraction, a pattern can be seen, of which the slope of the initial front determines the velocity of the MSPa. The slope is computed by

manually fitting a line (Fig. 3c, white dotted line) to the isoveLOCITY front of the wave. To reduce the variability resulting from manual tracking, as previously described for naturally occurring shear waves (Strachinaru *et al.* 2017, 2019), we compared this slope with the line between the entrance and exit points (frames) of the wave into the M-mode map (Fig. 3c, black dotted line). The entrance and exit points were also adjusted by frame-to-frame analysis. The velocity V of the MSPa is calculated, from the time T , which is the interval between the time stamps of the entrance and exit frames in the map, and the pre-defined M-mode length L , as $V = L/T$ in units of meters per second.

The length L ranged from 4 to 6 cm (4.9 ± 0.4 cm), starting from the onset of the muscular IVS (Fig. 3b). Propagation velocity was averaged over at least 3 heartbeats for every subject, randomly chosen from the three recorded clips.

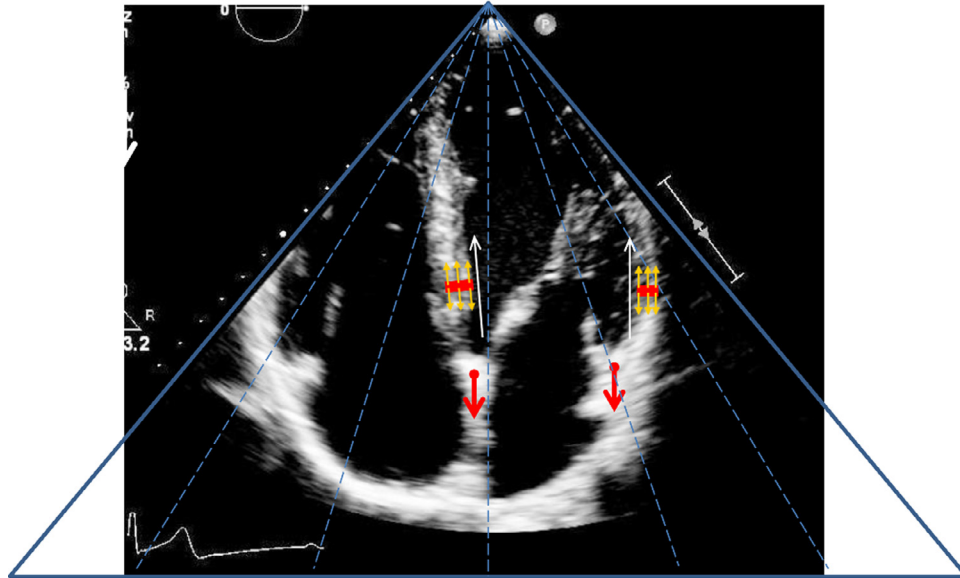


Fig. 2. Tissue motion as visible in the left ventricular walls after the atrial contraction, in the apical four-chamber view. Atrial contraction pulls on the mitral annulus (*red arrows*); this induces a local stretch (*small yellow arrows*) which propagates along the walls (*white arrows*) in the form of a tissue Doppler imaging pattern (*red line*). Note that the direction of the ultrasound in the apical view (*blue lines*) is in line with both the stretch and the direction of propagation.

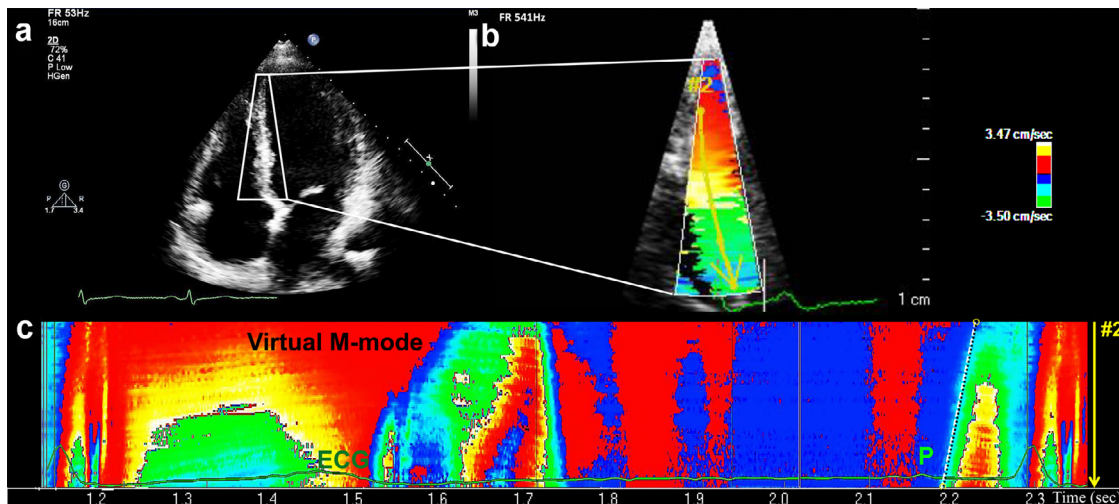


Fig. 3. Data obtained in the study patients using offline processing (modified to include one entire heartbeat). (a) Classical echocardiographic apical image and the focus region for high-frame-rate imaging. (b) High-frame-rate tissue Doppler imaging window over the interventricular septum. The M-mode line is traced midwall, ending at the beginning of the muscular septum, pointing toward the possible wave source. (c) Tissue Doppler imaging space–time map at 541 Hz, collected over the M-mode line of (b), of a full heart cycle (reconstructed offline). This map illustrates the wave-like velocity pattern after atrial contraction (P wave on the echocardiogram). The slope of the MSPa is traced along the isovelocity front (*white dotted line*) and compared with the line between the entrance and exit points (*yellow circles, black dotted line*) of the MSPa along the M-mode line. ECG = echocardiogram; MSPa = myocardial stretch post-atrial contraction.

Speckle tracking of the high-frame-rate 2-D data, represented as velocity vector imaging, was used in Qlab 9 to qualitatively determine the direction and propagation of local motion/deformation of the IVS after the atrial contraction. Anatomic M-mode tracings were also

obtained from the same grayscale data along the IVS using a general post-processing platform (Tomtec Imaging System 4.6, Unterschleissheim, Germany). They were also employed for qualitative comparison with the data from the TDI recordings.

Statistical analysis

Distribution of data was checked by using histograms and Shapiro–Wilk tests. Continuous variables were represented as the mean \pm standard deviation. Categorical data are presented as absolute number and percentage. For comparison of normally distributed continuous variables, we used the dependent or independent means *t*-test when appropriate. In case of a skewed distribution of continuous variables, the Mann–Whitney U-test was applied. For comparison of frequencies, the χ^2 -test or Fisher's exact test was used. Correlations were estimated using Pearson's correlation coefficient. The relationship between variables was investigated using univariate and multivariate regression models.

Each statistical analysis was performed using the Statistical Package for Social Sciences, Version 21 (IBM SPSS Statistics for Windows, Armonk, NY, USA). Testing was done two-sided and considered significant if the *p* value was <0.05 .

RESULTS

High-frame-rate tissue Doppler

The group characteristics and results are outlined in Table 1. There were significant differences in age, systolic blood pressure, septal thickness, e' , a' , a' acceleration and E/e' .

In the apical view, wave-like tissue velocity patterns were visible in all patients upon atrial contraction. In the parasternal longitudinal view of the LV, the grayscale traction movement of the IVS with atrial contraction was visible in all patients (Supplementary Video S1, online only), but high-frame-rate TDI could not visualize a wave phenomenon. This indicates that the dominant direction of tissue motion was along the septum, in line with the traction of the atria on the LV wall through the atrioventricular annulus.

In normal individuals and some HCM patients (Fig. 4a) the straight line corresponding to the entry–exit points of the MSPa into the M-mode line was superimposed on the first isovelocity trace (as described under Methods), revealing a globally constant propagation velocity. The same constant velocity is visible on the high-frame-rate virtual M-mode of the underlying 2-D data (Fig. 4b). Yet, we noticed in a substantial group of HCM patients ($n = 14$) that the MSPa isovelocity front had a non-constant propagation as evidenced by a deviation of more than two frames' time (3–4 ms) at any point along the first isovelocity tracing from the straight entry–exit line used for reference (Fig. 5): a first mild slope in the basal IVS, followed by a very steep slope in the mid-IVS (Fig. 5a). By use of M-mode tracings from the underlying 2-D data, the same behavior was confirmed (Figs. 5b and 7). In the case of such non-constant

propagation velocity, quantification was done in two ways. The average slope was quantified by computing the slope of the entry–exit points line as described under Methods (see Fig. 5a for an example), thus ignoring the deviation of the slope from a straight line. Alternatively, we manually traced the slowest and fastest first isovelocity slopes visible in the TDI panels (Fig. 5a, 1 and 2), and separately reported the slowest and highest apparent propagation velocities.

When analyzing the measured slope under the assumption of a linear propagation velocity (Fig. 6), the average velocity of the MSPa did not differ between normal volunteers (1.6 ± 0.3 m/s, range = 1.1–2.1 m/s) and the HCM patients (1.8 ± 0.8 , range = 0.9–3.8 m/s, $p = 0.14$). However, the maximum slope in the HCM patients presenting the non-constant TDI slope was 6.1 ± 3.4 m/s (range 2.3–12.5 m/s), which was significantly different from that of the normal volunteers ($p < 0.0001$). The slow slope in these patients was 1.4 ± 0.5 m/s (range = 0.8–2.5 m/s, $p = 0.2$) versus normal volunteers.

Subgroup analysis (Table 1, Fig. 6) among the patients with or without constant propagation velocity of the MSPa revealed a significant difference in septal thickness between the two groups (19 ± 4 mm in the non-constant propagation group and 16 ± 3 mm in the linear group, $p = 0.02$). Also, the linearized MSPa velocity in the non-constant velocity group was significantly higher than that in normal volunteers (2.6 ± 0.8 m/s vs. 1.6 ± 0.3 m/s, $p < 0.0001$).

The only parameter predicting the presence of a non-constant propagation velocity (Table 2) in a univariate and multivariate logistic regression analysis was the septal thickness ($p = 0.03$ univariate and $p = 0.001$ multivariate).

In the total group of 33 HCM patients, the linearized MSPa velocity did not correlate with age ($p = 0.24$), systolic or diastolic blood pressure ($p = 0.75$ and 0.96 , respectively), septal thickness ($p = 0.11$), e' ($p = 0.39$) or E/e' ($p = 0.47$).

The a' velocity and acceleration were significantly higher in the normal volunteers, suggesting either a stronger atrial traction on the mitral annulus or a stiffer IVS.

2-D tissue tracking and M-mode

The grayscale clips were analyzed with speckle tracking and anatomic M-mode, and for normal volunteers, local velocity vectors revealed a traction movement on the mitral annulus, followed by a local downward-only stretch, progressing from base to apex, later followed by a global outward movement of the whole IVS (atrial “volume kick”). As exemplified in Supplementary Video S2 (online only) and Figure 7a, in

Table 1. General characteristics and results in the study population (comparisons between groups and subgroups)

Parameter, units	Normal volunteer		HCM patients total		HCM patients with non-constant MSPa (A)		HCM patients with linear MSPa (B)		p A vs. B
	N = 42	N = 33	p vs. Normal	N = 14	p vs. Normal	N = 19	p vs. Normal		
Age, y	35 ± 14	49 ± 13	0.0001*	46 ± 14	0.01	50 ± 12	0.0002*	0.4	
Male sex	29 (69%)	24 (73%)	0.7	12 (85%)	0.3	12 (63%)	0.8	0.2	
BMI	24 ± 3	27 ± 5	0.002*	28 ± 5	0.0007*	26 ± 5	0.06	0.3	
Systolic blood pressure, mmHg	117 ± 12	131 ± 17	<0.0001*	135 ± 14	<0.0001*	127 ± 17	0.01*	0.2	
Diastolic blood pressure, mmHg	72 ± 7	76 ± 11	0.06	78 ± 10	0.028*	75 ± 11	0.2	0.4	
Septal thickness, mm	8 ± 1	17 ± 4	<0.0001*	19 ± 4	<0.0001*	16 ± 3	<0.0001*	0.02*	
Frame rate pulsed wave TDI, Hz	167 ± 17	197 ± 65	0.005*	197 ± 75	0.02*	196 ± 57	0.004*	0.9	
e', cm/s	8.3 ± 1.3	5.5 ± 1.9	<0.0001*	5.6 ± 1.7	<0.0001*	5.4 ± 2.1	<0.0001*	0.8	
E/e'	8 ± 1	16 ± 7	<0.0001*	16 ± 5	<0.0001*	16 ± 8	<0.0001*	1	
a', cm/s	8.6 ± 1.9	7.6 ± 1.8	0.02*	7.7 ± 2.2	0.15	7.5 ± 1.3	0.03*	0.7	
a' acceleration, cm/s ²	0.14 ± 0.04	0.10 ± 0.04	0.0001*	0.10 ± 0.05	0.004*	0.10 ± 0.04	0.0006*	1	
Frame rate color TDI, Hz	542 ± 30	530 ± 20	0.052	522 ± 22	0.03*	536 ± 16	0.4	0.04*	
Linearized MSPa (range), m/s	1.6 ± 0.3 (1.1–2.1)	1.8 ± 0.8 (0.9–3.8)	0.14	2.6 ± 0.8 (1.3–3.8)	<0.0001*	1.4 ± 0.4 (0.9–2.2)	0.03*	<0.0001*	
First slope MSPa (range), m/s	—	—	—	1.4 ± 0.5 (0.8–2.5)	—	—	—	—	
Second slope MSPa (range), m/s	—	—	—	6.1 ± 3.4 (2.3–12.5)	—	—	—	—	

BMI: body mass index; HCM: hypertrophic cardiomyopathy; MSPa: myocardial stretch propagation post atrial contraction.

Variables are presented as mean ± standard deviation

* Significant *p* values.

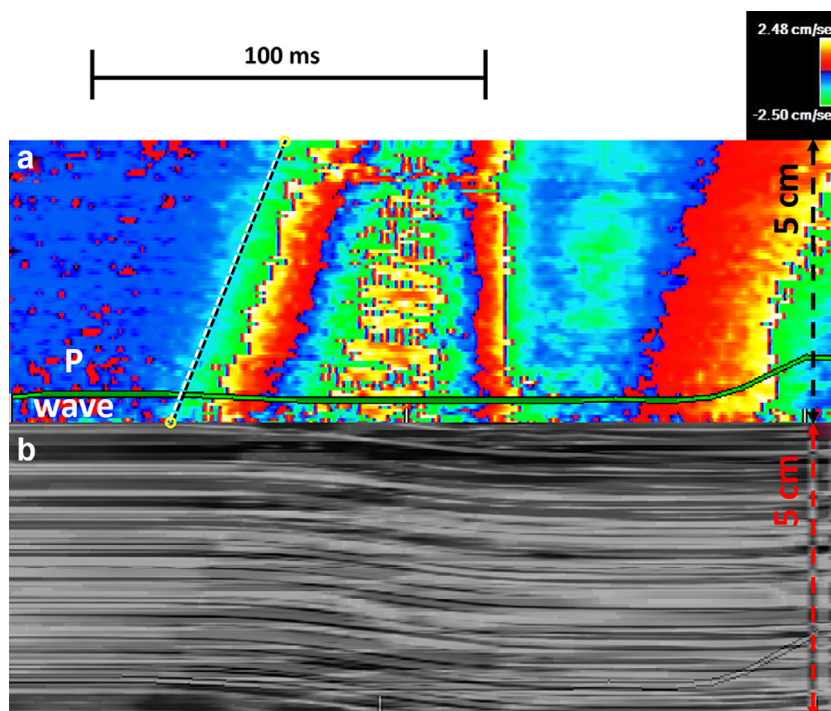


Fig. 4. Zoomed-in view of the end-diastolic phase after atrial contraction (P wave). (a) Tissue Doppler imaging velocity pattern starting from the basal interventricular septum. In normal volunteers and some hypertrophic cardiomyopathy patients, the isovelocities front line (*white dotted line*) was superimposed on the *black dotted line* traced between the entry and exit points of the myocardial stretch post-atrial contraction (yellow circles) into the M-mode map, revealing a constant slope. (b) Synchronous anatomic M-mode of the underlying 2-D information along the same M-mode line. A progressive base-to-apex downward line shift is visible, following the same contour.

HCM patients with a constant velocity of the initial front, the same progressive base-to-apex downward stretch could be seen. In patients having a non-constant velocity, we noticed after the mitral annulus traction an initial basal-only slow downward stretch, followed by a global rigid downward motion of the entire IVS and later a short outward movement (Supplementary Videos S3 and S4). This is consistent with the behavior of the MSPa in TDI and M-mode panels (Fig. 7b).

DISCUSSION

The main findings of this prospective study are as follows: (i) No significant difference could be found in the linearized propagation velocity of the wave-like pattern occurring in TDI post-atrial contraction between normal volunteers and HCM patients. (ii) Clinical and classic echocardiographic parameters did not correlate with the linearized propagation velocity of this pattern. (iii) In about half of the HCM patients, the wave front seemed to propagate with non-constant velocity, and this effect was related to disease severity as reflected by the end-diastolic septal thickness.

Previous studies have described the wave-like phenomena appearing in color TDI after atrial contraction (Pislaru *et al.* 2014, 2017; Voigt *et al.* 2002). By using a multimodality (speckle tracking, M-mode, TDI) approach, we found that the dominant direction of local tissue motion within the wave pattern was longitudinal to the wave propagation direction, as illustrated by the absence of the wave pattern in a parasternal TDI recording. When this study was compared with Voigt *et al.* (2002), there was a significant difference in the reported propagation velocity range, which could be due to errors in manually measuring very fast phenomena with relatively low time resolution in that study. In our study, the velocity range in normal individuals was similar to those found in earlier studies that used similarly high frame rates (Pislaru *et al.* 2014, 2017) but we could not find a statistically significant difference in linearized velocities between normal and pathologic myocardium, despite the numerous differences (age, body mass index and echocardiographic parameters) between the two study groups. This was an unexpected finding as HCM ventricles were considered a pathologic model of increased muscle stiffness and diastolic dysfunction (Elliott *et al.* 2014; Mirsky and Parmley 1973; Villemain *et al.* 2018a,

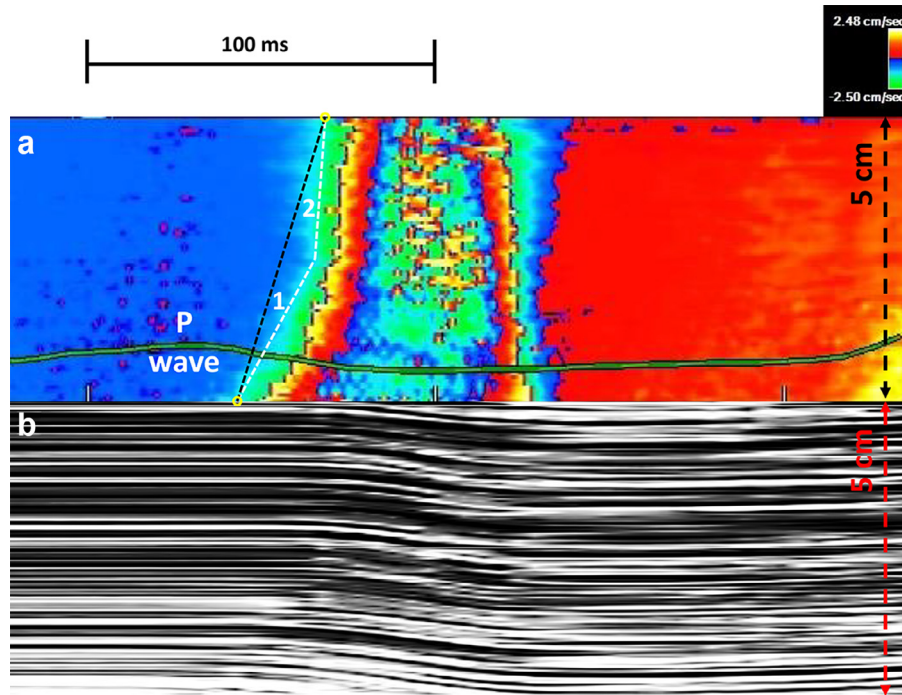


Fig. 5. In more than 40% of the patients with hypertrophic cardiomyopathy, a non-constant shape of the initial front could be seen. (a) Tissue Doppler imaging velocity pattern. The straight line between the entry and exit points of the MSPa into the M-mode map (*black dotted line*) emphasizes the deviation of the first isovelocity front (*white lines*) from a constant propagation velocity. The first milder slope is marked '1' and the second steeper slope is marked '2'. (b) Anatomic M-mode of the underlying 2-D information along the same M-mode line, revealing the same variation in propagation velocity.

b). Also, the linearized propagation velocity of this wave-like pattern was not correlated with differences in blood pressure, septal thickness or echographic signs of diastolic dysfunction. These findings differ from the results of previous studies (Pislaru et al. 2014, 2017). This triggered the in-depth analysis of TDI and 2-D data in search of an explanation.

We noticed the non-constant propagation of the front of the IVS deformation pattern post-atrial contraction, present in 42% of the HCM group, and this finding was statistically related to the septal thickness. Its appearance in the TDI map consists of a first mild slope (1.4 ± 0.5 m/s) in the basal part of the IVS followed by a very steep or almost vertical slope (Figs. 5 and 7) toward the apex, with an average velocity of 6.1 ± 3.4 m/s, which is much higher than the velocities measured in the group of healthy volunteers. Strikingly, the linearized MSPa velocity did not significantly differ between the two groups. On the other hand, it was significantly different when comparing only the non-constant velocity subgroup and normal volunteers (2.6 ± 0.8 m/s vs. 1.6 ± 0.3 m/s, $p < 0.0001$). This would suggest that only those patients with non-constant velocity propagation of the MSPa had higher myocardial stiffness than normal individuals. However, the two HCM groups

were statistically similar, except for the septal thickness (19 ± 4 vs. 16 ± 3 mm, $p = 0.02$).

With respect to this very steep slope, although HCM is associated with higher myocardial stiffness, such high propagation velocities have not been measured with an alternative stiffness measurement that uses induced shear waves by (Villemain et al. 2018a,b). They measured an average velocity of 3.5 m/s in the diastolic phase for HCM patients, which is a factor of 2 less than our average values in the steep slope. One explanation might be related to the physics of such traveling waves. The pulling action of the atria on the ventricle induces a wave in which the particle motion is mainly in the direction of its propagation (*i.e.*, along the wall), as also observed by the absence of a TDI wave pattern in the parasternal view. Such waves might behave as symmetric Lamb waves, as opposed to asymmetric Lamb waves or bulk shear waves which are generated with the technique applied by (Villemain et al. 2018a,b). The symmetric zero-order Lamb waves have a higher propagation velocity than bulk shear waves, up to a factor between 1.7 and 2 for a frequency range of nearly 0–40 Hz, as estimated by a wall thickness of 1 cm and propagation speed of 2 m/s (Brum 2019). Hence, the MSPa, purely because of its dominant longitudinal tissue

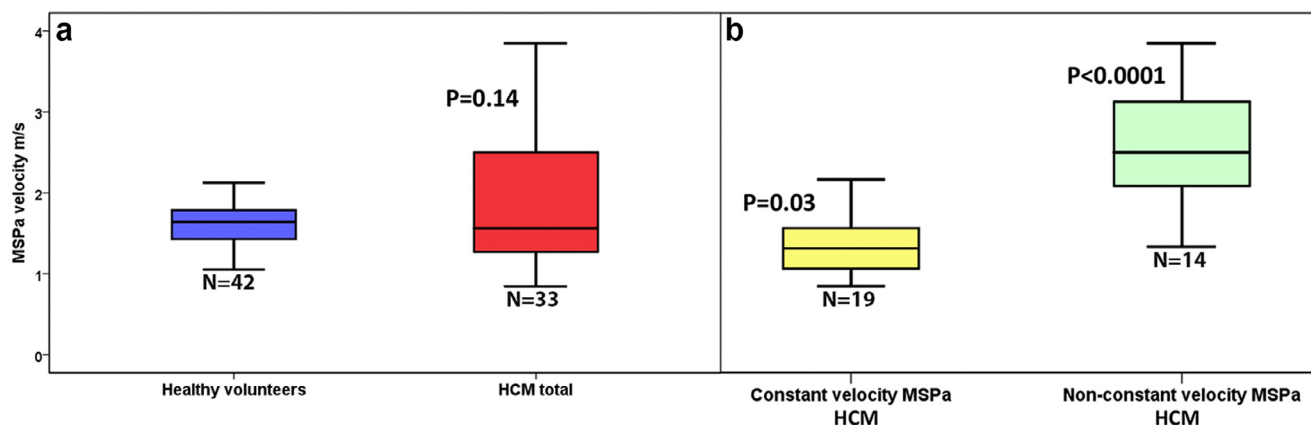


Fig. 6. Linearized propagation velocity of the MSPa in the study population of normal volunteers and HCM patients. (a) Comparison between normal volunteers and the whole HCM group. Although the velocity range is larger in HCM, the difference remains statistically non-significant. (b) By splitting the HCM according to the constant or non-constant velocity of the MSPa, we obtain two subgroups. The subgroup with constant-velocity MSPa has a slightly lower linearized MSPa than normal volunteers (1.4 ± 0.4 m/s, $p = 0.03$), whereas the non-constant velocity group has a significantly higher linearized propagation velocity (2.6 ± 0.8 m/s, $p < 0.0001$). HCM = hypertrophic cardiomyopathy; MSPa = myocardial stretch post-atrial contraction.

Table 2. Logistic regression analysis of the parameters predicting a non-constant propagation of the MSPa in HCM patients (N = 33)

Parameter	Univariate analysis		Multivariate analysis	
	95% CI	<i>p</i>	95% CI	<i>p</i>
Age	0.93–1.03	0.41	0.88–1.03	0.22
Sex	0.05–1.66	0.16	0.20–11.39	0.68
BMI	0.94–1.24	0.31		
Systolic blood pressure	0.98–1.08	0.21	1.01–1.20*	0.02*
Septal thickness	1.03–1.61*	0.03*	1.19–2.01*	0.001*
e'	0.73–1.48	0.84		
E/e'	0.91–1.11	0.97		

BMI: body mass index; CI: confidence intervals; MSPa: myocardial stretch post-atrial contraction.

* Significant *p* values.

motion direction, would expectedly lead to propagation velocities higher than those found by Villemain *et al.*, but it is very unlikely that they would reach well over 10 m/s.

(Villemain *et al.* 2018a,b) mentioned that the stiffness was measured in diastole, but it is unclear whether the measurement was timed before, during or after the atrial contraction. This timing may be critical, as experimental studies of the *ex vivo* myocardium have found an exponential relation between stress and strain (Holzapfel and Ogden 2009; Mirsky and Parmley 1973; Villari *et al.* 1993; Weber 1989). Atrial contraction in end-diastole leads to a rapid increase in LV strain, which might thus result in a rapid increase in momentary stiffness in the case of HCM, especially when the myocardium is close to its maximum distensibility. On slow-motion 2-D videos (Supplementary Videos S1–S4

at 220–250 Hz), the progression of the local tissue stretch after atrial contraction can be directly seen, as can its relation to the global displacement of the left ventricular wall. In normal volunteers (Fig. 3), the LV wall never reaches the maximal possible tissue distension permitted by the stiffer collagen network (Elliott *et al.* 2014; Weber 1989), allowing a progressive linear tissue stretch from base to apex. In the HCM patients in whom the slope was linear, some tissue distensibility may be preserved, and the LV stretch behaves similarly to that of normal individuals (Figs. 4 and 7a; Supplementary Video S2). In the more severe HCM patients, as the IVS becomes thicker and more rigid, the atrial contraction could induce a limited slow basal stretch, followed by a very steep movement of the entire LV wall as the hypertrophic ventricle reaches maximal longitudinal distension allowed by the collagen network (Figs. 5 and 7b; Supplementary Videos S3 and S4). In other words, the non-constant propagation would be caused by the shift from the myocardial stiffness to the stiffness of the limiting and more rigid collagen network surrounding the myocardial fibers. Depending on the degree of tissue distension existing before the atrial contraction, this shift may occur sooner or later, explaining the pattern in Figures 5 and 6, as well as the rigid wall motion seen in Supplementary Videos S3 and S4. Loading conditions will affect the strain of the myocardium and thus could drastically alter the propagation velocity of the MSPa (Voigt *et al.* 2002).

With respect to the initial mild slope, we discuss two possible explanations. First, the local stiffness of the basal septum could be lower than that of other parts of the septum, and similar to healthy tissue. Yet, this is less

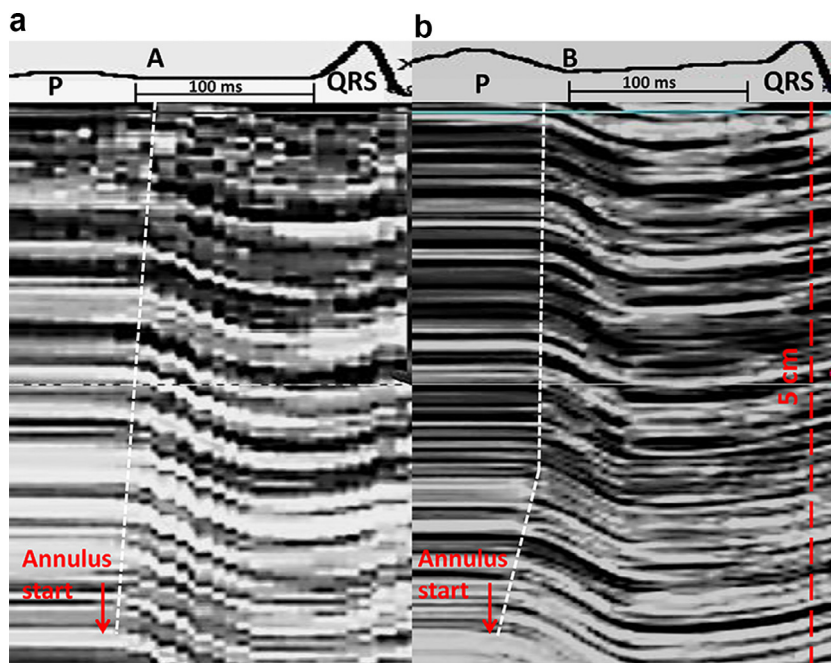


Fig. 7. Magnified zoomed-in view of anatomic M-mode tracings along the interventricular septum, at 250 Hz, over 5 cm, just after the start of the echocardiogram P wave and before the onset of the next QRS complex. The annulus is marked with a red arrow. (a) HCM patient with a linear MSPa velocity slope. The downward tissue shift as seen propagating along the M-mode line also follows a straight line (dotted line). (b) HCM patient exhibiting non-constant velocity of the MSPa. The first tissue downward motion has an initial milder slope, followed by a very steep one along the M-mode line. HCM = hypertrophic cardiomyopathy; MSPa = myocardial stretch post-atrial contraction.

likely in HCM, where muscle stiffening is expected to be diffuse. Second, if the tissue is indeed reaching a maximum distension during the atrial kick, then it would still be in an elastic state at the onset of the atrial kick, with its associated baseline stiffness values. Table 1 outlines a non-significant difference in the linearized propagation velocity of MSPa in the entire HCM group compared with healthy volunteers. On the other hand, if the HCM group is split on the presence of the non-constant propagation velocity, the difference between the two HCM subgroups is significant (2.6 ± 0.8 m/s vs. 1.4 ± 0.4 m/s, $p < 0.0001$), as is that between the non-constant propagation and the healthy volunteer group (2.6 ± 0.8 m/s vs. 1.6 ± 0.3 m/s, $p < 0.0001$). We also noted that HCM patients had a significantly lower a' velocity in pulsed TDI, as well as a lower a' acceleration slope. This finding could be interpreted as a lower and slower traction on the basal septum, potentially resulting in a slower basal stretch through viscous effects. This slower basal stretch remains directly visible in grayscale motion (Supplementary Video S4).

As for the possible transversal component, we expected this to be visible in the parasternal window in TDI (particle vibration in line with the Doppler), as already found for naturally occurring shear waves

(Strachinaru et al. 2017). But in our patients, no wave-like pattern could be seen in parasternal TDI after atrial contraction. From this observation we conclude that the dominant motion is a longitudinal stretch along the septal wall.

In 2-D imaging, the longitudinal stretch (MSPa) is shortly followed by an outward displacement of the whole LV wall, explained by the pressure rise in the ventricle after atrial contraction, which is called the volume stretch (atrial “volume kick”) and visualized by velocity vector imaging (Supplementary Videos S2 and S3). As it occurs later in time, that phenomenon is separate from the MSPa, which we consider in this study, and therefore out of the scope of the present study.

Limitations

High-frame-rate imaging represents a compromise between spatial and temporal resolution. The error in velocity estimation for very fast phenomena is larger with higher propagation velocity, lower frame rate and shorter traveling distance. A wave traveling at 2 m/s needs 25 ms to travel over a 5-cm length. At 5 m/s this time is reduced to 10 ms, and at 10 m/s, to 5 ms. At a frame rate of 540 Hz, the time resolution is a little less than 2 ms, which is sufficient to detect the general

behavior of the MSPa in normal individuals, but the error may be significant for velocities >10 m/s (see error analysis in Strachinaru *et al.* 2017, Appendix 1). Higher frame rates and averaging over multiple measurements would increase the accuracy of the propagation velocity measurements, which may be needed for actual clinical application.

The significance of our findings is limited by the number of patients. However, the non-constant propagation velocity was present in about half the patients even in this small group of HCM patients. Age matching was initially proposed for checking group variances, but was no longer considered, given the absence of statistically significant difference for the linearized MSPa between the study groups, despite their heterogeneity.

Tissue Doppler imaging velocities are known to be subject to angle dependency and cannot differentiate local deformation from global displacement (Dandel *et al.* 2009). Angle dependency was a minor issue in the TDI signal of the IVS in apical view because the motion was parallel to the ultrasound beam (Fig. 2). The absence of differentiation between local and global displacement was overcome by also studying tissue motion over the anatomic M-mode and by 2-D image analysis. Those measurements confirmed the findings from the TDI analysis.

As in previous studies, tracking of the MSPa was performed manually, which may increase the variability in velocity estimation, but to reduce this variability we traced a straight reference line between the entry and exit points of the MSPa into the M-mode map in all patients and adjusted it by frame-to-frame analysis as described under Methods. This line acted also as reference for the possible deviation of the MSPa from linearity.

Clinical implications and future directions

Analyzing the MSPa provides deeper insight into the diastolic function of the LV, as our findings suggest that the LV wall of HCM patients in diastole rapidly reaches a point where further longitudinal straining is constricted by the stiffer collagen network.

Because the MSPa does not exhibit the typical properties of an oscillatory shear wave, direct calculation of elasticity stiffness from its propagation velocity should be done with caution. Most likely, the propagation of the isovelocity front depends on the stress–strain relationship of the tissue, the actual strain during the atrial contraction, additional stresses caused by the LV loading conditions, and wall thickness, structure and geometry (Holzapfel and Ogden 2009; Villari *et al.* 1993; Voigt *et al.* 2002; Weber 1989). Therefore, calculating stiffness values from TDI measurements assuming a linear propagation velocity, as has been done in earlier

studies, may be an oversimplification and may miss clinically relevant deviations from this assumption. However, the presence of a non-linear MSPa seems to indicate more advanced disease in HCM, with a significantly thicker septum and presumably more fibrosis. Further research may be directed to using this as a qualitative sign of disease severity without the need to directly compute stiffness values.

CONCLUSIONS

The onset of the left ventricular end-diastolic myocardial stretch after atrial contraction exhibits a constant and quantifiable propagation velocity in normal individuals, but a non-constant velocity in about half of the HCM patients in the study. This deviation of the TDI velocity pattern can be explained by a non-linear relation between strain and stress and the inhomogeneous structure of the LV wall, even more apparent in thickened hypertrophic myocardium. This would imply clinical relevance, but actual quantification of tissue elasticity should be performed with care.

Acknowledgments—This work is part of the STW–Dutch Heart Foundation partnership program “Earlier Recognition of Cardiovascular Diseases,” Project No. 14740, which is (partly) financed by the Netherlands Organization for Scientific Research (NWO).

Conflict of interest disclosure—The authors declare that they have no conflict of interest.

SUPPLEMENTARY MATERIALS

Supplementary material associated with this article can be found in the online version at doi:10.1016/j.ultrasmedbio.2019.04.031.

REFERENCES

- Brekke B, Nilsen LC, Lund J, Torp H, Bjastad T, Amundsen BH, Stoylen A, Aase SA. Ultra-high frame rate tissue Doppler imaging. *Ultrasound Med Biol* 2014;40:222–231.
- Brun J. Transverse Wave Propagation in Bounded Media. In: Nenadic I, Urban M, Greenleaf J, Gennisson JL, Bernal M, Tanter M, (eds). *Ultrasound elastography for biomedical applications and medicine*. Hoboken, NJ: Wiley; 2019. p. 93–96.
- Cikes M, Tong L, Sutherland GR, D’hooge J. Ultrafast cardiac ultrasound imaging: Technical principles, applications, and clinical benefits. *JACC Cardiovasc Imaging* 2014;7:812–823.
- Dandel M, Lehmkuhl H, Knosalla C, Suram lashvili N, Hetzer R. Strain and strain rate imaging by echocardiography—Basic concepts and clinical applicability. *Curr Cardiol Rev* 2009;5:133–148.
- Elliott PM, Anastakis A, Borger MA, Borggrefe M, Cecchi F, Charron P, Hagege AA, Lafont A, Limongelli G, Mahrholdt H, McKenna WJ, Mogensen J, Nihoyannopoulos P, Nistri S, Pieper PG, Pieske B, Rapezzi C, Rutten FH, Tillmanns C, Watkins H. 2014 ESC Guidelines on diagnosis and management of hypertrophic cardiomyopathy: The Task Force for the Diagnosis and Management of Hypertrophic Cardiomyopathy of the European Society of Cardiology (ESC). *Eur Heart J* 2014;35:2733–2779.
- Giorgi H. *The physics of waves*. 171–197 Englewood Cliffs, NJ: Prentice Hall; 1993. p. 282–284.

- Holzapfel GA, Ogden RW. Constitutive modelling of passive myocardium: A structurally based framework for material characterization. *Philos Trans A Math Phys Eng Sci* 2009;367:3445–3475.
- Kanai H. Propagation of vibration caused by electrical excitation in the normal human heart. *Ultrasound Med Biol* 2009;35:936–948.
- Mirsky I, Parmley WW. Assessment of passive elastic stiffness for isolated heart muscle and the intact heart. *Circ Res* 1973;33:233–243.
- Pernot M, Couade M, Mateo P, Crozatier B, Fischmeister R, Tanter M. Real-time assessment of myocardial contractility using shear wave imaging. *J Am Coll Cardiol* 2011;58:65–72.
- Pislaru C, Pellikka PA, Pislaru SV. Wave propagation of myocardial stretch: Correlation with myocardial stiffness. *Basic Res Cardiol* 2014;109:438.
- Pislaru C, Alashry MM, Thaden JJ, Pellikka PA, Enriquez-Sarano M, Pislaru SV. Intrinsic wave propagation of myocardial stretch, a new tool to evaluate myocardial stiffness: A pilot study in patients with aortic stenosis and mitral regurgitation. *J Am Soc Echocardiogr* 2017;30:1070–1080.
- Song P, Bi X, Mellema DC, Manduca A, Urban MW, Greenleaf JF, Chen S. Quantitative assessment of left ventricular diastolic stiffness using cardiac shear wave elastography: A pilot study. *J Ultrasound Med* 2016;35:1419–1427.
- Strachinaru M, Bosch JG, van Dalen BM, van Gils L, van der Steen AFW, de Jong N, Geleijnse ML, Vos HJ. Cardiac shear wave elastography using a clinical ultrasound system. *Ultrasound Med Biol* 2017;43:1596–1606.
- Strachinaru M, Bosch JG, van Gils L, van Dalen BM, Schinkel AFL, van der Steen AFW, de Jong N, Michels M, Vos HJ, Geleijnse ML. Naturally occurring shear waves in healthy volunteers and hypertrophic cardiomyopathy patients [e-pub ahead of print]. *Ultrasound Med Biol*. doi: <https://doi.org/10.1016/j.ultrasmedbio.2019.04.004>, Accessed May 10, 2019.
- Vejdani-Jahromi M, Freedman J, Nagle M, Kim YJ, Trahey GE, Wolf PD. Quantifying myocardial contractility changes using ultrasound-based shear wave elastography. *J Am Soc Echocardiogr* 2017;30:90–96.
- Villari B, Campbell SE, Hess OM, Mall G, Vassalli G, Weber KT, Kraysenbuehl HP. Influence of collagen network on left ventricular systolic and diastolic function in aortic valve disease. *J Am Coll Cardiol* 1993;22:1477–1484.
- Villemain O, Correia M, Khraiche D, Podetti I, Meot M, Legendre A, Tanter M, Bonnet D, Pernot M. Myocardial stiffness assessment using shear wave imaging in pediatric hypertrophic cardiomyopathy. *JACC Cardiovasc Imaging* 2018a;11:779–781.
- Villemain O, Correia M, Mousseaux E, Baranger J, Zarka S, Podetti I, Soulat G, Damy T, Hagège A, Tanter M, Pernot M, Messas E. Myocardial stiffness evaluation using noninvasive shear wave imaging in healthy and hypertrophic cardiomyopathic adults [e-pub ahead of print]. *JACC Cardiovasc Imaging* 2018b; doi: [10.1016/j.jcmg.2018.02.002](https://doi.org/10.1016/j.jcmg.2018.02.002). Accessed November 23, 2018.
- Voigt JU. Direct stiffness measurements by echocardiography: Does the search for the holy grail come to an end? [e-pub ahead of print] *JACC Cardiovasc Imaging*. doi: <https://doi.org/10.1016/j.jcmg.2018.02.004>, Accessed 9 March 2018.
- Voigt JU, Lindenmeier G, Werner D, Flachskampf FA, Nixdorff U, Hatle L, Sutherland GR, Daniel WG. Strain rate imaging for the assessment of preload-dependent changes in regional left ventricular diastolic longitudinal function. *J Am Soc Echocardiogr* 2002;15:13–19.
- Vos HJ, van Dalen BM, Heinonen I, Bosch JG, Sorop O, Duncker DJ, van der Steen AF, de Jong N. Cardiac shear wave velocity detection in the porcine heart. *Ultrasound Med Biol* 2017;43:753–764.
- Weber KT. Cardiac interstitium in health and disease: The fibrillar collagen network. *J Am Coll Cardiol* 1989;13:1637–1652.